

## Three-dimensional reconstruction of heliospheric structure using iterative tomography: A review

B.V. Jackson<sup>a,\*</sup>, P.P. Hick<sup>a,b</sup>, A. Buffington<sup>a</sup>, M.M. Bisi<sup>a,c</sup>, J.M. Clover<sup>a</sup>, M. Tokumaru<sup>d</sup>,  
M. Kojima<sup>d</sup>, K. Fujiki<sup>d</sup>

<sup>a</sup> Center for Astrophysics and Space Sciences, University of California, San Diego, 9500 Gilman Drive # 0424, La Jolla, CA 92093-0424, USA

<sup>b</sup> San Diego Supercomputer Center, University of California, San Diego, 9500 Gilman Drive #0505, La Jolla, CA 92093-0505, USA

<sup>c</sup> Institute of Mathematics and Physics, Aberystwyth University, Penglais Campus, Aberystwyth, Ceredigion, SY23 3BZ Wales, GB

<sup>d</sup> Solar-Terrestrial Environment Laboratory, Nagoya University, Furo-cho Chikusa-ku, Nagoya, Aichi 464-8601, Japan

### ARTICLE INFO

#### Article history:

Received 31 March 2010

Received in revised form

30 September 2010

Accepted 11 October 2010

Available online 28 October 2010

#### Keywords:

Three-dimensional heliospheric density and velocity reconstructions

Solar wind flows

Interplanetary coronal mass ejections

### ABSTRACT

Current perspective and in-situ analyses using data from NASA's twin Solar TERrestrial Relations Observatory (STEREO) spacecraft have focused studies on ways to provide three-dimensional (3-D) reconstructions of coronal and heliospheric structure. Data from STEREO are preceded by and contemporaneous with many other types of data and analysis techniques; most of the latter have provided 3-D information by relying on remote-sensing information beyond those of the near corona (outside 10  $R_S$ ). These include combinations of past data from the Helios spacecraft and the Solwind coronagraphs and, continuing from the past to the present, from observations of interplanetary scintillation (IPS) and the Solar Mass Ejection Imager (SMEI) instrument. In this article we review past and ongoing analyses that have led to a current great wealth of 3-D information. When properly utilized, these analyses can provide not only shapes of CME/ICMEs but also a characterization of any solar wind structure or global outflow.

© 2010 Elsevier Ltd. All rights reserved.

### 1. Introduction

Current perspective analyses of data from the NASA's twin Solar TERrestrial Relations Observatory (STEREO) spacecraft (Kaiser et al., 2008) have focused coronal and heliospheric studies on ways to extract three-dimensional (3-D) tomographic information about the corona and inner heliosphere from remote-sensing views. Others (e.g., Mierla et al., 2010) have reviewed many of the techniques used in these 3-D analyses, and we do not repeat this review. While the STEREO in-situ and remote-sensing data themselves are unique (e.g., Galvin et al., 2008; Harrison et al., 2009), they grew out of much past analysis and coincide with a great body of contemporaneous work by many researchers. These include analyses of interplanetary scintillation (IPS) observations from as long ago as e.g., Hewish et al. (1964) or Houminer (1971), and of Thomson-scattering brightness data (photospheric sunlight scattered by electrons) from the Helios spacecraft photometers, the Solwind coronagraph (Jackson et al., 1985), the Large Angle Spectrographic Coronagraphs (LASCO) (Brueckner et al., 1995) on board the Solar and Heliospheric Observatory (SOHO) (Domingo et al., 1995), and finally the Solar Mass Ejection Imager (SMEI)

instrument (Eyles et al., 2003; Jackson et al., 2004) on board the Coriolis spacecraft.

Numerous attempts have been made to reconstruct the corona and heliosphere in three dimensions. Near the Sun there is a strong motivation to determine the 3-D shapes of coronal structures in order to learn about their initiation and source of energy. Coronal mass ejections (CMEs) often have a loop-like appearance when viewed with a coronagraph. If these helical loops are driven by currents as proposed early-on by Anzer (1978) and Mouschovias and Poland (1978), the shape of a CME should follow a very specific pattern. If instead a CME is a spherical bubble, then it might very well be the remnant of a large addition of energy at a single point in the low corona (Wu et al., 1976). Various techniques used to determine CME shapes from the single perspective of Earth include polarization of transient structures (Munro 1977; Crifo et al., 1983; reviewed in Wagner, 1984), and are more recently presented by Moran and Davila (2004). Depletions of the corona and an estimation of the minimum line of sight (LOS) length for three CMEs (MacQueen, 1993) also gave an indication that CMEs are extensive coronal structures. Studies using multiple different-vantage-point perspectives from the Helios spacecraft photometer remote-sensing observations and the Solwind coronagraph reached the same conclusion (Jackson et al., 1985). The extent and the shape of structures in the background corona are also important. For instance, the shapes and positions of coronal streamers indicate their location and extents relative to the magnetic structures

\* Corresponding author. Tel.: +1 858 534 3358; fax: +1 858 534 0177.  
E-mail address: [bjackson@ucsd.edu](mailto:bjackson@ucsd.edu) (B.V. Jackson).

on the Sun. This in turn indicates whether coronal streamers are formed by the effects of a global solar-current “pinch” effect or some more local magnetic phenomenon. Studies of the solar wind and the processes supplying its energy can only be carried out if a global description of the solar wind is available.

Forecasting in heliospheric physics requires both remote-sensing data and analyses that measure evolving 3-D morphologies of solar and interplanetary structures. In the case of flares and other large-transient changes near the solar surface this information can predict both whether that structure will erupt and given that it does, whether it will subsequently affect Earth. This premise, more than any other, has promoted the 3-D analyses of remote-sensing data from ground-based IPS, or spaceborne SMEI or STEREO instruments. In the following article, most of the analyses of eruptive events are provided by white-light Thomson-scattering observations, and for simplicity we refer to these as CMEs, rather than using the term ICME or a combination of CME/ICME in following these events to their interplanetary manifestation.

Section 2 gives a background of some of the early work utilizing both the IPS and Thomson-scattering observations to provide 3-D tomography from heliospheric data sets. This early work inspired current tomographic-analysis techniques, which assume little other than the physical principles of plasma outward flow, in order to derive the shapes of outward-flowing heliospheric structures. Section 3 gives a brief background of the particular techniques used by the University of California, San Diego (UCSD) and Solar-Terrestrial Environment Laboratory (STELab) Nagoya University Japan groups for this tomographic analysis. Section 4 gives recent results and compares these different analysis techniques. We conclude in Section 5.

## 2. Analyses prior to 2005

When global remote-sensing heliospheric data are available, several types of Computer Assisted Tomography (CAT) are available that reconstruct the co-rotating and outward-flowing solar wind by making use of the rearrangement of features along each LOS. These analyses generally assume no a priori information about the structures mapped except that they follow the general physical principles assumed for heliospheric outward flow, and that their LOS weighting can be readily calculated. For most versions of the UCSD STELab tomography analyses, for instance, radial outward propagation of the solar wind and conservation of mass and mass flux for different-speed solar wind structures is assumed (e.g., see Jackson et al., 1998).

### 2.1. Early IPS and Thomson-scattering analyses

Since the 1960s IPS has been used to probe solar wind features using ground-based meter-wavelength radio observations (Hewish et al., 1964; Houminer, 1971). Intensity-scintillation IPS observations, arising from small-scale ( $\sim 150$  km) density variations, show heliospheric disturbances of larger scale that vary from 1 day to the next and are often associated with geomagnetic storms (Gapper et al., 1982). These disturbances are present in the solar wind, emanate from only certain regions on the Sun, and are often found to be associated with the onset of high speed solar wind in near-Earth spacecraft measurements. As inferred from a list of events, their shapes, and their solar surface associations during observations from 1978 to 1979 (Hewish and Bravo, 1986) mapped these disturbances to the solar surface and concluded the only common identifiable surface feature to be coronal holes observed in He I 10830 Å maps. Observations from the UCSD (Coles and Kaufman, 1978) and STELab (Kojima and Kakinuma, 1987) multi-site scintillation array systems have determined velocities in the interplanetary medium since the early 1970s. Fig. 1a shows an IPS radio array currently operating in Japan, that as one of three antenna systems now operating, has provided nearly continuous heliospheric observations in real time since the mid-1990s. All antennas operate simultaneously to view one radio source at a time as it transits the central meridian above Japan in order to measure the scintillation level and the transit time of the scintillation pattern across the Earth surface (see Fig. 1b). The transit time of the scintillation pattern allows a determination of solar wind velocity perpendicular to the line of sight for each radio source viewed, as well as an independently determined scintillation-level measurement from each system that views the source.

Significant results have been obtained from IPS remote-sensing observations even with only a rudimentary locating of solar-wind structures along each LOS, i.e., the assumption that all material is at the LOS's closest location to the Sun. For instance, from IPS velocity data it was determined that the polar solar wind has high speed (Kakinuma, 1977; Coles et al., 1980; Kojima and Kakinuma, 1990) long before the Ulysses spacecraft (Phillips et al., 1994; McComas et al., 1995) measured these velocities in situ. Especially at solar minimum, regions of slow solar wind are generally found near the solar equator, and thus also near the magnetic-neutral line (“current sheet”) as determined by the potential-magnetic-field model (Hoeksema et al., 1983). Scintillation level data from the Cambridge 81 MHz array have been analyzed in the same manner (e.g., Hick et al., 1995). Carrington maps produced by assuming the solar wind at the LOS location closest to the Sun show that the near-solar polar

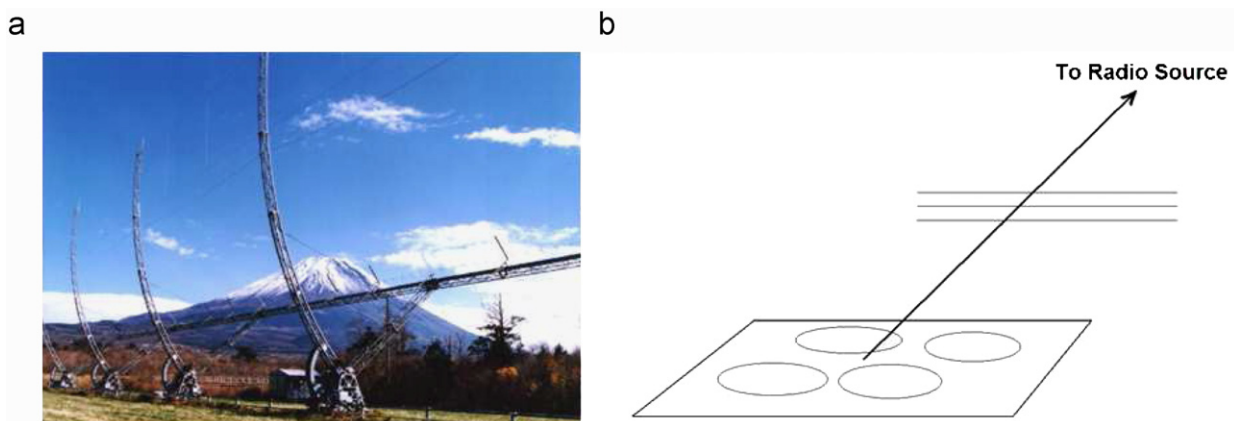


**Fig. 1.** (a) STELab IPS radio array at a frequency of 327 MHz (one of three now operating in Japan) near Mt. Fuji. The arrays each measure scintillation intensity (or  $g$ -value) for about 40 radio sources each day. Scintillation signals when cross-correlated between arrays provide a robust IPS velocity determination. (b) A depiction of the  $\sim 150$  km size scintillation intensity pattern on the surface of the Earth produced by interplanetary scintillation. Motion of this pattern across the Earth's surface produces intensity variations used to determine solar wind velocity and density variation.

regions generally do not scintillate strongly compared to regions near the solar equator. *Houminer and Gallagher (1993)* find that some of the regions which both scintillate strongly and co-rotate (return from one rotation to the next) are located near the heliospheric current sheet. *Hick et al. (1995)* determined that solar active regions generally bright in X-rays, and not the current sheet, are the associated solar surface locations of most co-rotating structures observed to scintillate strongly in the Cambridge IPS data.

Tomography of transient heliospheric structures using global IPS data has often been attempted without the aid of sophisticated computer techniques. These analyses (*Gapper et al., 1982; Behannon et al., 1991*) have relied on a combination of solar rotation, outward motion and in-situ measurements to determine the 3-D extent of coronal structures. In these analyses with Cambridge data, different 3-D coronal-structure models were transformed to a two-dimensional image “template”. These templates were then matched by eye to the observation to select the model best representing the data. A continuing and more sophisticated approach (*Tokumaru et al., 2003a, b, 2006*, see Section 4) assumes model structures and iterates parameters to fit several-day sequences of IPS data. These analyses of transient structures continue to the present.

The first truly remote-sensing heliospheric-imaging white-light data came from the zodiacal-light photometer experiments on the twin Helios spacecraft. Two Helios spacecraft were launched: the first in December 1974, and the second in January 1976. Their photometers were designed to map the brightness of the zodiacal dust cloud to an unprecedented precision, as viewed from their unique orbits (*Leinert et al., 1975, 1981a, 1981b*), carrying the spacecraft between 0.3 and 1.0 AU in the ecliptic plane with a 6-month period. The sky was mapped in 65 heliographic locations at 16°, 31°, and 90° ecliptic latitude, and in three color bands using a rotating filter wheel which also had three polarization orientations and a clear filter (e.g., *Leinert et al., 1982; Leinert and Pitz, 1989*). Limited by a downlink data rate of only one bit per second, the total sample interval extended over approximately 5 h. Because absolute photometry was a major goal, both photometers and the Helios spacecraft themselves were designed to keep stray light to a minimum (where other instruments up to that time had failed; see *Leinert and Klüppelberg, 1974*). An essential feature for tomographic analysis was this instrument’s ability to obtain a many-day Thomson-scattering brightness change (which in turn provides a good proxy for heliospheric density change) since, if present, variable stray light could otherwise overwhelm the faint variable Thomson-scattering signal.

Helios photometers detected “plasma clouds” (*Leinert et al., 1982*) that were traced in several examples by *Richter et al. (1982)* to CMEs observed by the Solwind coronagraph (*Sheeley et al., 1980*). The Helios spacecraft spin axis perpendicular to the ecliptic plane enabled Helios 1 photometers to view to the south, and Helios 2 to the north. Sky coverage retained enough spatial information to provide CME images over nearly half a hemisphere (*Jackson, 1985a, b; Jackson and Leinert, 1985*) from its non-Earth viewpoint. Among other notable achievements, these images tracked a halo CME (as observed from Earth) outward along the Sun–Earth line from the perspective of the two spacecraft, until it produced a geomagnetic storm (*Jackson, 1985a*). They also provided perspective information about the 3-D shapes of CMEs (e.g., *Jackson et al., 1985, 1988*), and a determination of the density enhancements behind heliospheric shocks (*Jackson, 1986*). These same white-light observations were also used to view co-rotating heliospheric structures and to measure their outflow and persistence (*Jackson, 1991*).

## 2.2. Early heliospheric tomographic analyses

Tomography is best known for its application in the medical profession, where it provides a non-invasive way to probe the

human body, and reconstruct its internal 3-D structure (see *Gilbert, 1972*, for one of the first uses). Even earlier, however, tomography was used in solar radio astronomy (*Bracewell, 1956*). Tomographic reconstruction techniques have also been successfully applied in binary-star-system studies (*Marsh and Horne, 1988*), astrophysical accretion disk studies (*Gies et al., 1994*), acoustic sounding in oceanography (*Worcester et al., 1991*), seismic studies in geology (*Anderson and Dziewonski, 1984*), auroral studies (*Frey et al., 1996*), and solar coronal studies (*Hurlburt et al., 1994*). An application in atmospheric modeling, somewhat similar to our present model in its use of an irregular sampling of refractometric sounding observations is discussed in *Gorbunov (1996)*. In general, the final 3-D resolution depends upon the individual-exposure resolution and noise, and the number of available perspective views. In medical applications it is generally possible to obtain as many different views and directions as required for the high-resolution 3-D measurement of tissue and bone. Most of the other tomographic applications are limited by an inability to view objects from a large number of directions.

Some of the first coronal tomographic analyses using Skylab coronagraph data (*Wilson, 1977; Jackson, 1977*) employed solar rotation to provide perspective views of the corona. *Zidowitz et al. (1996)* carried this approach further in the mid-1990s, using rotational tomographic techniques to reconstruct coronal densities from Mark III coronagraph data. Later co-rotational tomography of SOHO UVCS data (*Panasyuk, 1999; Frazin, 2000; Frazin and Janzen, 2002*) showed considerable improvement over analyses that previously had simply assumed that the structure is on the limb at the time of observation. An even more recent version of this technique has been applied to coronal observations from STEREO and SOHO that relaxes the co-rotational assumption somewhat (*Butala et al., 2010*). A two-perspective-view tomographic analysis of CMEs by *Jackson and Hick (1994)* and *Jackson and Froehling (1995)* using Solwind coronagraph and Helios photometer data also showed the extended 3-D shapes of two CMEs.

The techniques described here apply CAT methods to data primarily obtained from one location in space. Thompson-scattering LOS weighting was incorporated from coronal studies (*Billings, 1966*) and used in an early article for heliospheric observations covering a large range of solar elongations (angular distances from the Sun) in *Jackson et al. (1988)*. This and subsequent analyses in the late 1980s and early 1990s (*Jackson and Hick, 1994; Jackson and Froehling, 1995*) combined views from the Solwind coronagraph and Helios spacecraft photometers, and expanded CME structure radially and self-similarly outward from near the Sun to distant from it. The LOS weighting somewhat different than that for Thomson scattering, and appropriate for IPS was first presented in early articles by *Kojima et al. (1996, 1997, 1998)*, *Jackson et al. (1997b, 1998)*, and *Asai et al. (1998)*. Co-rotational analyses using these techniques improved upon the inherent averages made previously by assuming all material lies at the point of closest approach of the LOS to the Sun. Results covering an extended period of time provide a global view of the inner heliosphere, and both solar rotation and outward solar wind motion provide the multiple perspectives required for the tomographic analyses. Selecting data for the co-rotational analysis from a quiet part of the solar cycle minimizes evolution effects during the period of observation.

In the present context, iterative tomography reconstructs a set of model parameters from a “source surface” or inner boundary which are propagated outward to define a 3-D heliospheric model of density and/or velocity. This is then compared with observations at each LOS. Parameters are adjusted to match as closely as possible the LOS integrated model to the remotely-sensed observations. A time-dependent version of this tomographic technique from a single point in space (as in *Jackson et al., 2001, 2003*), relaxes the assumption that heliospheric structure remains constant over

time. In this case, a global heliospheric model is updated at regular time intervals, and the iterative process provides the 3-D (two spatial coordinates over time) parameters on source surfaces that fit heliospheric data observed at different times. These latter analyses permit reconstruction that accommodates temporal variations in the data. If the shortness of these time steps is small enough, this ensures that perspective views of the data come from outward motion of solar wind plasma rather than solar rotation.

These tomographic analyses, with IPS data as input, have been available since the early 2000s to provide 3-D heliospheric reconstructions from the STELab radio-array data, and are used to forecast co-rotating and transient heliospheric structure during the portion of the year when these arrays operate (generally from April to December each year). Plans are now underway to use one of these arrays for year-around operation. These analyses and visualizations are found on the Web at <http://ips.ucsd.edu/> (USA), and <http://stesun5.stelab.nagoya-u.ac.jp/index-e.html/> (Japan).

The time-dependent tomographic analysis was used more recently to provide 3-D heliospheric density reconstruction using Helios photometer observations alone. Although no coronagraph data exist during the period in November 1977, the period has been well-studied using in-situ data from five different spacecraft (Burlaga et al., 1980; Fig. 2a). Fig. 2b–d presents remote-observer views from a 3-D reconstruction using the Helios data from this time period. The density reconstruction satisfactorily depicts both the co-rotating structure and an assumed CME piston that was postulated using in-situ measurements. Other examples of this

tomographic analysis using early Helios data is found in Jackson and Hick (2005) and Jackson et al. (2001), and was first announced in Jackson and Hick (2000).

### 3. Current UCSD and STELab tomographic heliospheric analyses

The majority of 3-D reconstruction techniques from both UCSD and STELab groups are exploratory, in that few assumptions are made about the heliospheric-structure shapes other than that they follow the general physical principles of outward heliospheric flow, and that the LOS response is appropriately weighted. For the UCSD analysis a kinematic solar wind model is propagated outward assuming conservation of mass and mass flux. This allows a determination of whatever structure may be present without any further assumptions imposed beyond the above physical principles. It also provides a “hands free” solution to this determination, so that data analyses and even forecasts do not rely on human intervention once the initial programming is set up. Finally, the technique is used to improve data analysis and data inputs from different measurement techniques, and to remove noise from these inputs at the different times the analyses are performed. Further details are presented elsewhere (Jackson et al., 1998, 2008b, 2010b; Kojima et al., 1998; Asai et al., 1998; Jackson and Hick, 2002; Hick and Jackson, 2004), and are outlined briefly below for the two current techniques.

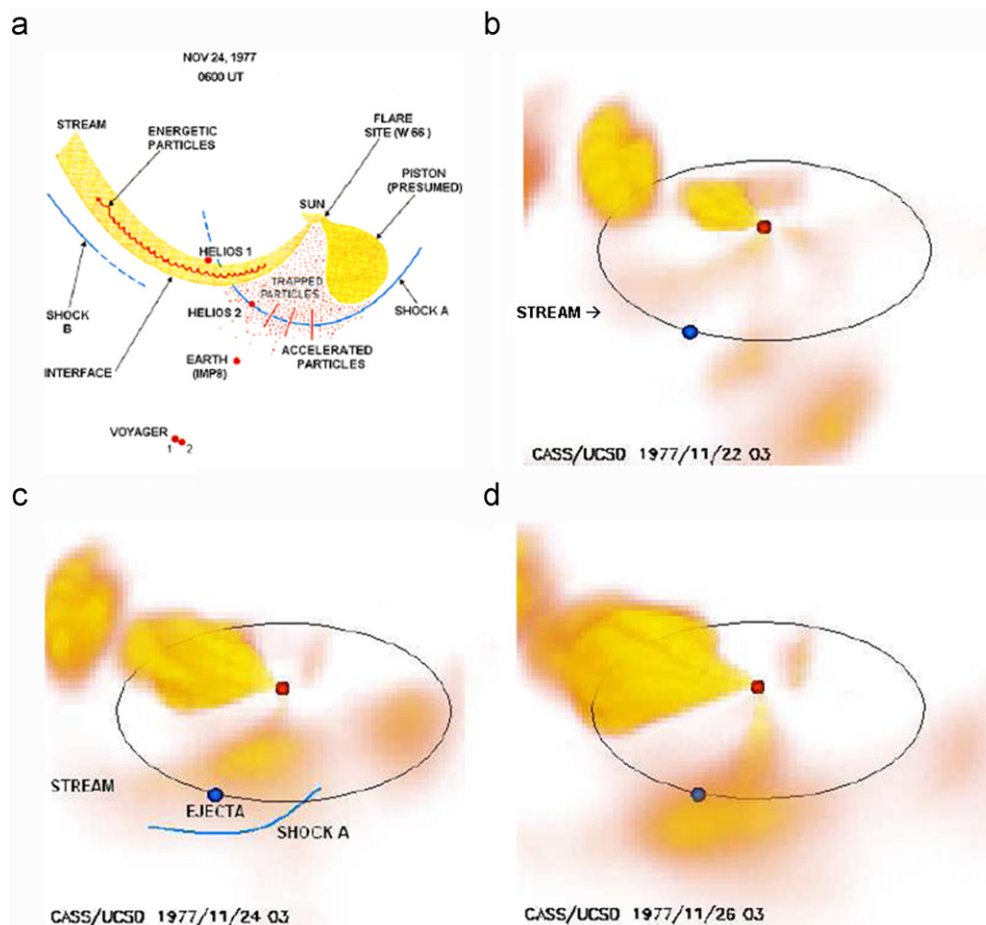


**Fig. 2.** (a) Heliospheric analysis at 06:00 UT 24 November 1977, from in-situ measurements with five spacecraft (Burlaga et al., 1980). (b–d) Remote observer views from a composite of both Helios 1 and 2 photometer data using the time-dependent Thomson-scattering tomography. The progression of the stream and ejecta are observed over the 5-day interval. The observer is located  $30^\circ$  above the ecliptic  $\sim 20^\circ$  west of the Sun–Earth line. Earth is marked as a blue dot on its elliptical orbit.

The IPS LOS weighting function makes several assumptions that relates local changes in the scintillation level and velocity to changes in these values integrated along each LOS. In weak scattering (which is implicitly assumed for these IPS observations) the Born approximation holds true, and the resultant scintillation pattern at Earth is therefore a sum of contributions from each thin scattering layer perpendicular to the LOS (Tatarski, 1961). At any given radio frequency, this weak-scattering approximation breaks down at some solar elongation close to the Sun, and the scintillation level is no longer a sum of each scattering layer. Effectively optically thick, this region is no longer related in the same way as in thin scattering to bulk density. Depending on observing frequency and radio source size this effect limits how close to the Sun lines of sight can be used for 3-D reconstructions employing IPS observations.

Two different tomographic 3-D reconstruction programs were developed independently in the mid-1990s by the STELab group and by those at UCSD. These both require that a solar wind model be estimated by projecting model parameters outward from a source surface (or inner boundary) where they can be compared with each LOS observation. The model differences from the LOS observations are iteratively changed to fit observations according to weights appropriately assigned to each line segment (see Fig. 3) back-projected to the source surface. Use of a source surface makes the tomographic inversion a two-dimensional analysis, or a three-

dimensional inversion analysis (i.e., latitude, longitude, and time) in the case of the time-dependent tomography. This maximizes the use of the information from each LOS observation. As said previously, the contribution from each LOS segment consists of a weight determined from the IPS or Thomson-scattering process itself times a value from the solar wind structure (i.e., local density or velocity). These two factors for either IPS or Thomson-scattering signals are separable, thus allowing the LOS segment weights to be initially determined for each LOS, and the resulting contributions then modified appropriately by the heliospheric structure as the inversion proceeds.

Because the solar wind model is determined by source surface input parameters that are altered by the inversion technique, the solar wind model line-of-sight projections, weights, and differences from the steady observed values change significantly at each inversion. Thus in these analyses both the UCSD and STELab reconstruction programs are iterated to convergence from the original inputs provided on the source surface. In the UCSD 3-D reconstructions each iteration is monitored to determine a least squares variance between observed and modeled line of sight values, and the change of the initial source surface parameters. Tests of the program show that within a few iterations any knowledge of the original source surface input is lost, and that convergence is usually obtained within a few iterations. The STELab

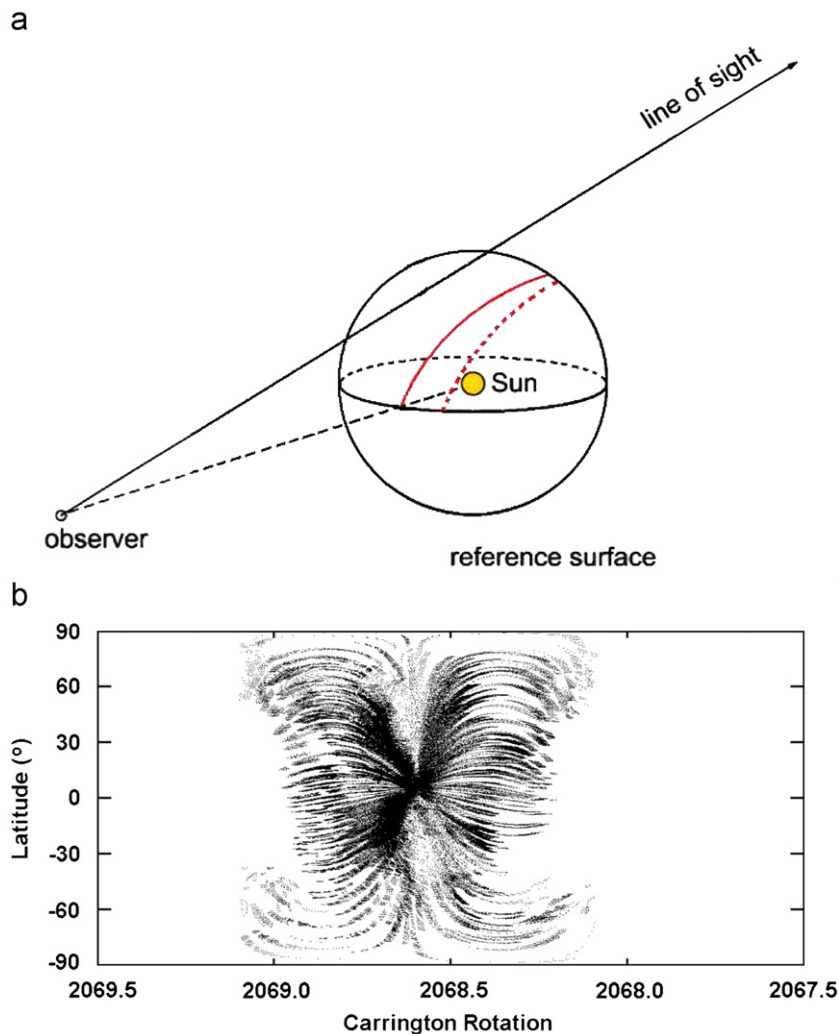


**Fig. 3.** (a) Depiction of a line of sight and its projection to the reference surface. The solid line is the immediate projection of the line of sight to this surface; the dashed line is the projected location that takes into account the solar wind speed. (b) Line-of-sight projections of SMEI data for a typical half day in the middle of Carrington rotation 2068. Lines of sight emanate from the projected location below the Earth, radiate outward from this point, and complete projected positions at adjacent times.

program iterations are generally monitored in a similar way. The reader is referred to Jackson et al. (1998) or Kojima et al. (1998) for a more complete discussion of these tests for the comparable co-rotating versions of the UCSD and STELab 3-D reconstruction programs.

The UCSD 3-D reconstruction program is available in two different versions; co-rotating and time-dependent. The co-rotational program assumes that the material viewed to the east and west of the Sun is the same, but viewed from a different perspective as the structure rotates past Earth (see Jackson et al., 1998). For the UCSD analysis it has been found that latitude and longitude resolutions near Earth can be reconstructed on considerably better than  $10^\circ \times 10^\circ$  latitude and longitude resolutions, and that at this resolution a whole Carrington rotation can be covered without locations left blank. The UCSD time-dependent program places a 1-day time step in the reconstructions, and assumes that each daily measurement at the source surface is unique. The formal inversion to convergence on the source surface for the time-dependent model utilizes only  $\sim 40$  observed radio sources per day, and the spatial resolution for this 3-D reconstruction near the Earth is subsequently reduced to latitude and longitude resolutions of  $20^\circ \times 20^\circ$  with a 1-day cadence. When a transient structure such as a heliospheric response to a CME is observed across a large range of solar elongations, it is viewed from widely different directions. This changing perspective that includes the weights ascribed to the changing structure viewed at different perspectives is exploited to reconstruct a 3-D time-dependent solar-wind model. Both the cadence and the spatial resolutions in the program can be varied to accommodate more (or fewer) lines of sight, but the lowest spatial resolutions are seldom set below this limit or at less than this cadence. From SMEI images there are nearly 40,000 lines of sight over the sky in each 102-min orbital map that can potentially be used for 3-D reconstructions. High energy particle hits, bright stars, aurora, and the computer processing required in removing these contaminant signals limit the effective LOS numbers the 3-D reconstructions can use. Typically the SMEI 3-D reconstructions use about 1000 lines of sight from each orbit, and both spatial and temporal resolutions for the time-dependent program can be greatly increased. This provides much finer spatial and temporal resolutions in the near-Earth vicinity and, on average, over the whole of the heliosphere accessed by the SMEI image data.

In the UCSD analyses, the inversion is provided on a fixed grid in latitude, longitude (and for the time-dependent tomography, also time) by combining lines of sight weighting that are nearest to each grid point. The weighting of nearest points is determined by a Gaussian filter that assigns contributions to a given grid point based on the distance of the projected line of sight segment to that point in spherical coordinates on the source surface relative to the point. If there are too few contributions or too little weighting to a grid point from nearby lines of sight, the grid point is not inverted tomographically. When these measurements are projected into the final volume presented, they are left blank. However, because these blank areas could provide an incomplete estimate of the total line of sight effect, following the inversion points in the matrix are smoothed by an additional set of Gaussian filters, and at the final step this filtering is used to completely fill the matrix. This is accomplished in latitude and longitude on the source surface for the co-rotating analysis, and in latitude, longitude, and time for the multiple source surfaces of the time-dependent tomography. In the UCSD kinematic solar wind model that is formed from the source surface parameters and propagated outward to provide a comparison with observations, both mass, and mass flux are conserved. This kinematic modeling step was deemed necessary to provide an accurate solar wind model for the far more abundant Thomson-scattering SMEI data where a high resolution near Earth is desirable.

The comparable STELab 3-D reconstruction program is available in only one version; co-rotating, and is not available for Thomson-scattering measurements. In this 3-D reconstruction program, the digital resolutions used for STELab data are somewhat finer in latitude and longitude than in the UCSD IPS co-rotating version, and the line of sight effect is formed by distributing each line of sight measurement and weighting over many different grid points on the source surface, and not simply the nearest one. In this program the solar wind model does not conserve mass or mass flux, and this is sufficiently accurate for the very low daily numbers of lines of sight in the STELab IPS analysis. Tests of this technique show extremely good comparable results to the co-rotating IPS analysis from UCSD.

We refer the reader to further comprehensive discussions of the UCSD 3-D reconstruction analysis for both IPS measurements (Jackson et al., 1998, 2003, 2008b; Hick and Jackson, 2004; Bisi et al., 2010a, 2010b) and Thomson-scattering measurements (Jackson et al., 2001, 2006, 2008a, 2008b; Jackson and Hick, 2005; Bisi et al., 2008a). The STELab IPS reconstruction technique that was developed independently (Kojima et al., 1998; Asai et al., 1998) has been used with further modification and changes to allow a 3-D MHD solar wind model kernel to propagate the source surface parameters outward (Hayashi et al., 2003a, 2003b). This version of the STELab co-rotational analysis is interpolated between 27-day Carrington rotation reconstructions to provide time-varying source surface solar wind speed inputs for an MHD solar wind model, but has not yet been used to iterate to convergence using the MHD model kernel. Other references to these tomographic analyses are found in Kojima et al. (2001, 2004, 2007).

The SMEI baffled cameras (Fig. 4a) were designed to provide data for an Earth-based system that optimizes the analysis of 3-D heliospheric structures located along the LOS to the Sun from Earth (Jackson et al., 2010c). The lines of sight used in SMEI tomographic analysis are chosen to be located distant from stellar positions brighter than 6th magnitude on a SMEI image that might cause suspect changing signals (Fig. 4b). Because (as for IPS observations) lines of sight from an Earth-orbiting instrument provide a maximum density of remote-sensing heliospheric information near the Earth, we expected the SMEI data to provide the most accurate 3-D reconstructions for structures passing close to the instrument (close to Earth). Fig. 5 indicates why this is true; not only are the numbers of lines of sight more numerous across the volume elements near the Earth but also the maximum response from the Thomson-scattered signal draws closer to Earth and becomes at the location of Earth as the viewing elongation extends to  $90^\circ$  and beyond (anti-sunward).

Unlike IPS, heliospheric Thomson-scattering along each LOS is optically thin at elongations from within a small fraction of a solar radius all the way out to  $180^\circ$  (completely anti-solar). The brightness signal is directly proportional to heliospheric electron number. However, unlike the IPS observations, Thomson-scattering brightness is small compared with the total observed surface brightness. At elongations of a few degrees Thomson-scattering brightness is at best only a few percent of the zodiacal light, and this percentage diminishes with greater elongations. Stellar signals are also hundreds of times brighter than the Thomson-scattering signal, and their potential removal is complicated by a very uneven distribution across the sky. The prior analyses from the Helios photometers (designed to measure zodiacal-light brightness) showed that the Thomson-scattering signal from an instrument in deep space varied sufficiently compared with background brightness contaminants to allow instruments of this type to measure heliospheric signals out to elongations greater than  $90^\circ$ . For SMEI, the variation of high-energy-particle hits on the CCD in Earth orbit was anticipated, and the variation of brightness of the geocorona (Meier and Mange, 1973; Anderson et al., 1987), and the

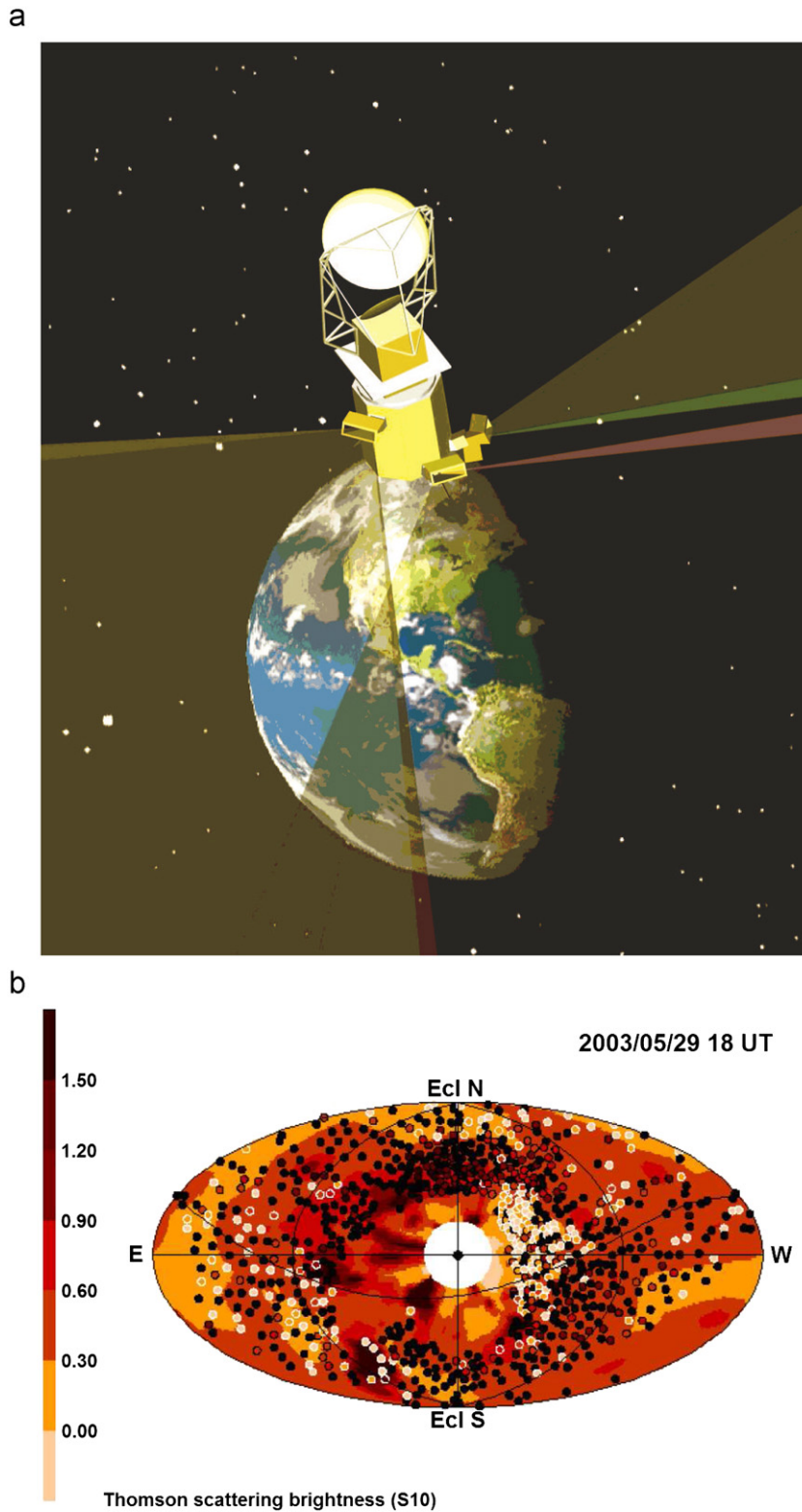


**Fig. 4.** (a) SMEI in its polar orbit at 840 km altitude with an orbital inclination of  $98^\circ$ . The Sun is to the left and the satellite moves over the terminator. SMEI looks away from the Earth at  $\sim 30^\circ$  from the local horizontal to avoid sunlight reflected from the Earth and from the Windsat antenna above it. The combined fields of view of the three cameras (shown as shaded cones) cover nearly all the sky. (b) A whole sky map in Hammer-Aitoff format obtained from SMEI images presented in S10, the equivalent brightness of a tenth magnitude solar-type star in one square degree of sky. The valid lines of sight within one 3-h period centered on the time of the image are shown. The color of the LOS indicates the brightness of an individual measurement, and is plotted against the iterated model value at the time indicated. The onset of an ICME event sequence that arrived at Earth on 30 May 2003 is shown (from Jackson et al., 2008a). (For interpretation of the references to color in this figure legend, the reader is referred to the web version of this article.)

brightness contamination from other spacecraft in the vicinity of the instrument have proven not difficult to remove from the measurements. Not known prior to SMEI launch was the brightness

of high-altitude auroral light above the instrument near the Earth's poles (Mizuno et al., 2005). Of the various contaminant signals specific to Earth orbit, only those from the aurora are particularly

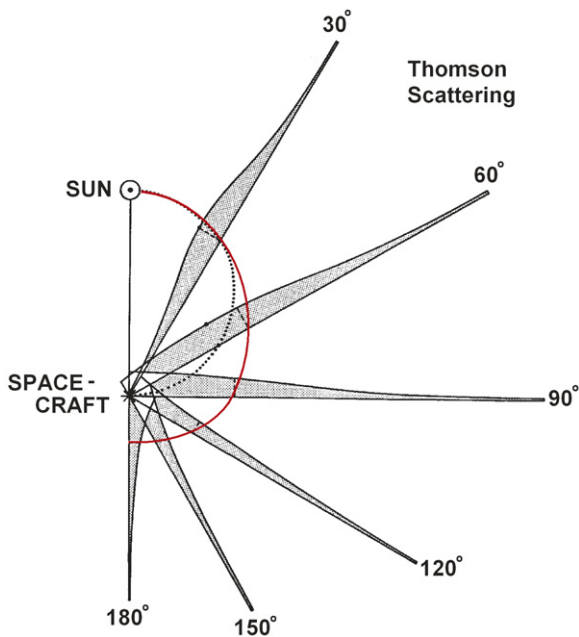


**Fig. 5.** Relative-response distribution of the Thomson-scattering brightness contribution along the LOS for an  $r^{-2}$  heliosphere. The point of closest approach to the LOS to the Sun is marked by the dotted line. The solid curve from the Sun shows the median location of the LOS response (from Jackson, 1985b), and has been used in previous articles as a rough means to estimate the distance to structures that have moved beyond  $90^\circ$  elongation.

difficult to accommodate in the SMEI data analysis. From the surface of the Earth, mesospheric air glow at even the darkest sites presents a time-variable signal that is several ten times larger (Garcia et al., 1997; James et al., 1997) than heliospheric signals. Mesospheric air glow has effectively limited ground-based or near-ground Thomson scattering observations to elongations within a few solar radii of the Sun, and the best of these have been obtained at times of total solar eclipses by instruments in high-flying aircraft (Chapman, 1979).

#### 4. Recent results and the comparisons of these different tomographic analysis techniques

Both the UCSD and STELab 3-D IPS analyses have provided reconstruction analysis results on the Web in real time since the year 2000. These can be compared for co-rotating results, and have a comparable ability to forecast heliospheric-structure arrival at the Earth. The tomographic analysis from the STELab group has been used recently in several comprehensive studies of global velocity throughout Solar Cycles 22 and 23 (Tokumaru et al., 2010). In these analyses the solar polar wind speed is measured and reconstructed globally, and contrasted to those speeds measured near the ecliptic plane.

As mentioned in Section 3, there as yet has been no time-dependent inversion technique developed by the STELab group for IPS data (Kojima et al., 2007). However, as also mentioned in Section 2, Tokumaru et al. (2003b, 2007) have developed a technique for analyzing the STELab IPS data that determines CME parameters by assuming a structure shape and iterating to find best fits of the structure parameters to the data. As an example, these analyses are compared in Fig. 6, and show four 3-D reconstructions of the 28 October 2003 CME, three at about the same time using the UCSD time-dependent technique with SMEI and IPS data from STELab, and another using the technique developed by the STELab group. Fig. 6a shows the density reconstruction using SMEI Thomson-scattering observations

combined with IPS velocity analyses (Jackson et al., 2006). Fig. 6b and d show this same time period reconstructed from the STELab IPS g-level data using the two different 3-D reconstruction techniques. In Fig. 6d, the technique developed by Tokumaru et al. (2003b, 2007) determines specific parameters for the loop-shaped CME using IPS data and the best model fitted iteratively to this shape. There are very few IPS sources to the South during this period of STELab observations, and in the structure there is an extrapolation from observed sources to the North on this day. In Fig. 6b, the UCSD technique employs both IPS g-level and velocity data to reconstruct the structure at the time given; since there is so little IPS information available to the South at this time, no structure to the South appears in this image. The structures to the North have about the same radial distance in Fig. 6a and b. Fig. 6c gives an overall view of the dense CME structure as it has expanded outward between the orbit of Earth and the orbit of Mars. Here, the dense region appears more loop-like. In Fig. 6b, the structure is highlighted when density is above  $10 \text{ e}^- \text{ cm}^{-3}$  to show the extent of the 3-D structure and above which the excess mass for the event is determined. To provide the calibration for this event, the same conversion factors used for the Bastille-day CME (14 July 2000) were used to reconstruct this CME (Jackson and Hick, 2005). To determine excess CME mass, the region above a defined contour level is approximated by cubes, and the mass within the total of these cubes is summed. The defined region also provides an ambient solar wind mass which in this instance is assumed to be associated with  $5 \text{ e}^- \text{ cm}^{-3}$  at 1 AU, and is scaled to higher values (using an  $r^{-2}$  density fall-off) at nearer distances to the Sun. The excess and total mass of the northern lobe of the 28 October 2003 CME determined from the UCSD 3-D reconstruction from SMEI for this event above the  $10 \text{ e}^- \text{ cm}^{-3}$  contour level is, respectively,  $6.8 \times 10^{16}$  and  $8.5 \times 10^{16} \text{ g}$  (Jackson et al., 2006). The excess and total mass determined for this same northern lobe from the UCSD IPS 3-D reconstruction of this CME event is, respectively,  $3.2 \times 10^{16}$  and  $4.5 \times 10^{16} \text{ g}$  (see Fig. 6d). Tokumaru et al. (2007) obtain a mass of  $6.5 \times 10^{16} \text{ g}$  for their analysis of the 28 October 2003 CME. In comparison, the plane-of-the-sky excess mass for this portion of the event from LASCO data is a rather small  $0.5 \times 10^{16} \text{ g}$ , but this needs to be multiplied by a significant factor ( $> 3 \times$ ) because the bulk of this northern portion of the halo CME is so distant from the plane of the sky. A more comprehensive accounting of the total and excess mass for the 28 October 2003 CME and its different parts using the SMEI instrument 3-D reconstructions is found in Jackson et al. (2006, 2007b).

The UCSD 3-D reconstruction technique can also be used to simultaneously reconstruct both STELab IPS velocities and densities from SMEI (Fig. 7). For the 28 October 2003 CME observed on 03:00 UT, 30 October 2003, the major dense portion of the CME that follows behind the shock response has an excess and total mass above the  $10 \text{ e}^- \text{ cm}^{-3}$  density contour level, respectively, of  $11.4 \times 10^{16}$  and  $14.2 \times 10^{16} \text{ g}$  (see Fig. 7a). These event totals do not encompass as much material as the analysis of the same event in Jackson et al. (2006), but agree within 20% of the earlier analysis. A high-velocity region ( $> 1000 \text{ km s}^{-1}$ ) precedes this dense mass to the east and west along the ecliptic behind the major shock response measured in situ near Earth. In determining total mass and energy associated with a CME event, one can simply sum the total excess mass observed or, since there is high-speed outward flow also associated with the CME response, this can be included in its mass and energy accounting. Fig. 7a estimates energy for the outward-flowing CME mass contained within the  $10 \text{ e}^- \text{ cm}^{-3}$  contour level to be  $4.5 \times 10^{32} \text{ erg}$ . To evaluate the high-speed flow component, excess and total CME mass contained within the  $900 \text{ km s}^{-1}$  contour interval for this event is found to be, respectively,  $1.0 \times 10^{16}$  and  $1.8 \times 10^{16} \text{ g}$  and these are an order of magnitude less than the masses determined just above. However, because this associated CME material moves outward so rapidly, the energy associated with this high-speed solar-wind flow (mapped in Fig. 7c) is found to be  $0.8 \times 10^{32} \text{ erg}$ , and thus a somewhat larger fraction ( $\sim 18\%$ ) of the total CME energy.

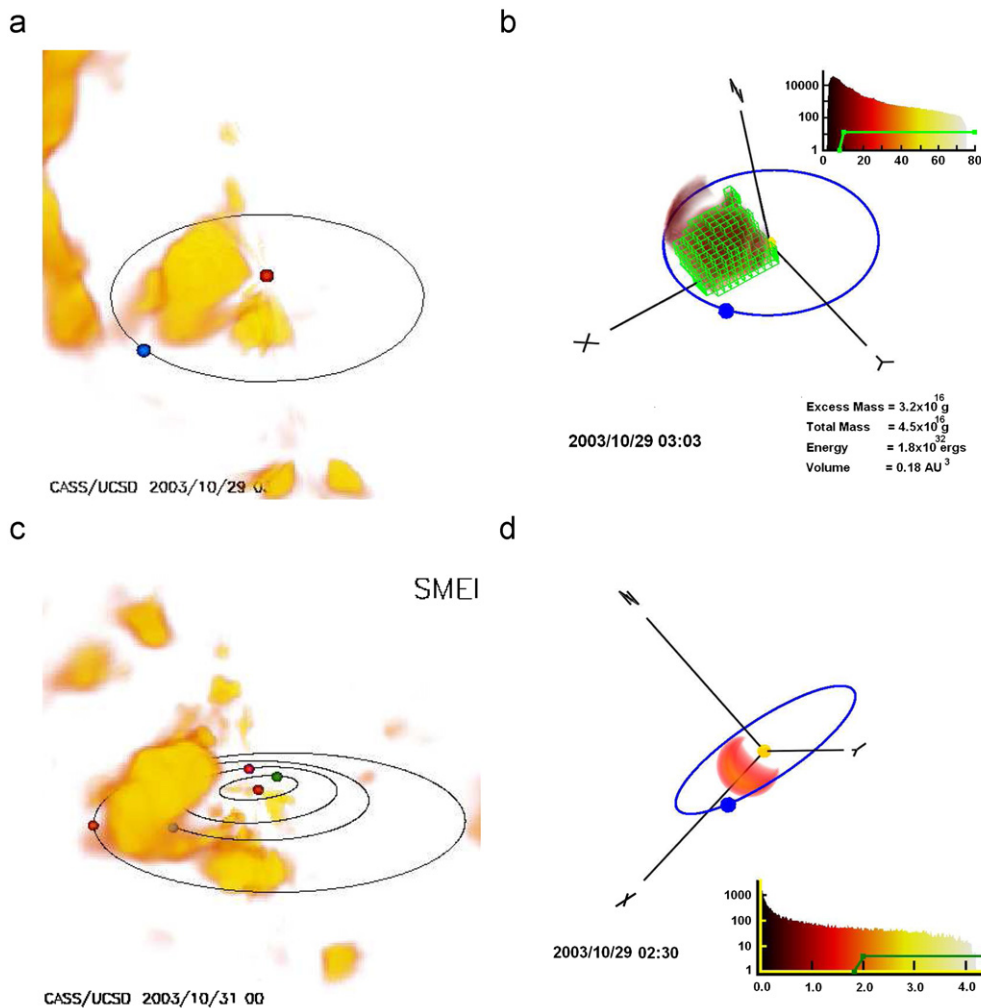


**Fig. 6.** (a) 3-D density reconstruction using Thomson-scattering SMEI observations, of the heliospheric response to the 28 October 2003 CME, as viewed from 3 AU at  $30^\circ$  above the ecliptic plane and  $45^\circ$  West of the Sun–Earth line. The Earth is indicated as a blue circle in its elliptical orbit; the Sun by a red circle at the center. Contours are from 10 to  $30 \text{ e}^- \text{ cm}^{-3}$  and have an  $r^{-2}$  density gradient removed normalized to 1 AU (from Jackson et al., 2006). (b) UCSD 3-D IPS reconstruction of the same event from  $g$ -level data. As in the SMEI analysis in (a), contours are shown upward from  $10 \text{ e}^- \text{ cm}^{-3}$  and also have an  $r^{-2}$  density gradient removed from the density analysis normalized to 1 AU. The dense structure to the solar West shown in Fig. 1d is not shown in this reconstruction. (c) UCSD SMEI 3-D density reconstruction of the same 28 October CME at a slightly later time showing its extent as the main portion of the ecliptic density has moved outward to between Earth and Mars. The orbits of all the inner planets are shown for scale. (d) STELab 3-D reconstruction in  $g$ -level of the 28 October 2003 CME (from Tokumaru et al., 2007). The Earth is again depicted on its orbit in blue. A histogram gives the range of  $g$ -levels depicted in the reconstruction. (For interpretation of the references to color in this figure legend, the reader is referred to the web version of this article.)

For the 28 October 2003 CME it is possible to determine the extent of the shock density enhancement that is present in front of the high-speed solar wind. In a recent development since the analysis presented in Jackson et al. (2006), a slightly higher-resolution reconstruction of CME density from SMEI allows shock density enhancements to be measured (Jackson et al., 2010a, under review). Fig. 8 shows these enhancements for the 28 October 2003 CME, presented for the first time in this review; this reveals a shock density enhancement that is neither continuous nor that forms a shell-like front at the edge of the high-speed solar wind region. This analysis shows, as do the results in Jackson et al. (2010a, under review), a CME shock response that varies greatly with location in front of the CME.

Comparisons between the 3-D reconstruction results and in-situ spacecraft measurements are important not only to provide a “ground truth” for these remotely-obtained results but also (having accepted the ground truth confirmation) to refine these results. Because we expect in-situ measurements to be more precise (and they are certainly available at a much higher temporal cadence), this comparison allows a refinement of remote-sensing data and reconstruction results. Comparison of 3-D reconstructed densities

and velocities using IPS data with in-situ measurements of these parameters has been successful since the year 2000 in real time using data from STELab, and is presented at both UCSD and STELab websites (as previously stated). The comparisons become even more successful when used with archival data sets, since these also include the remotely-sensed structure after they have passed beyond the observer. In a more recent development Jackson et al. (2010b) have incorporated in-situ measurements into the remotely-sensed IPS velocity time-dependent tomography. This is accomplished by including a heavily weighted in-situ measurement into the 3-D model at the location of Earth, and to iterate to convergence with observations using this additional constraint. This not only provides an extremely good match of the tomographic result with the in-situ measurements at the location and time input, but it also shows in forecasts that this significantly refines the overall remotely-sensed tomographic result.

Comparisons of these 3-D reconstruction results using the remote-sensing archival data sets with in-situ measurements is now a fairly routine matter. For IPS analyses these comparisons have been made near Earth for selected periods (e.g., Jackson et al., 1998, 2003; Dunn et al., 2005; Bisi et al., 2009a), at Mars (Jackson

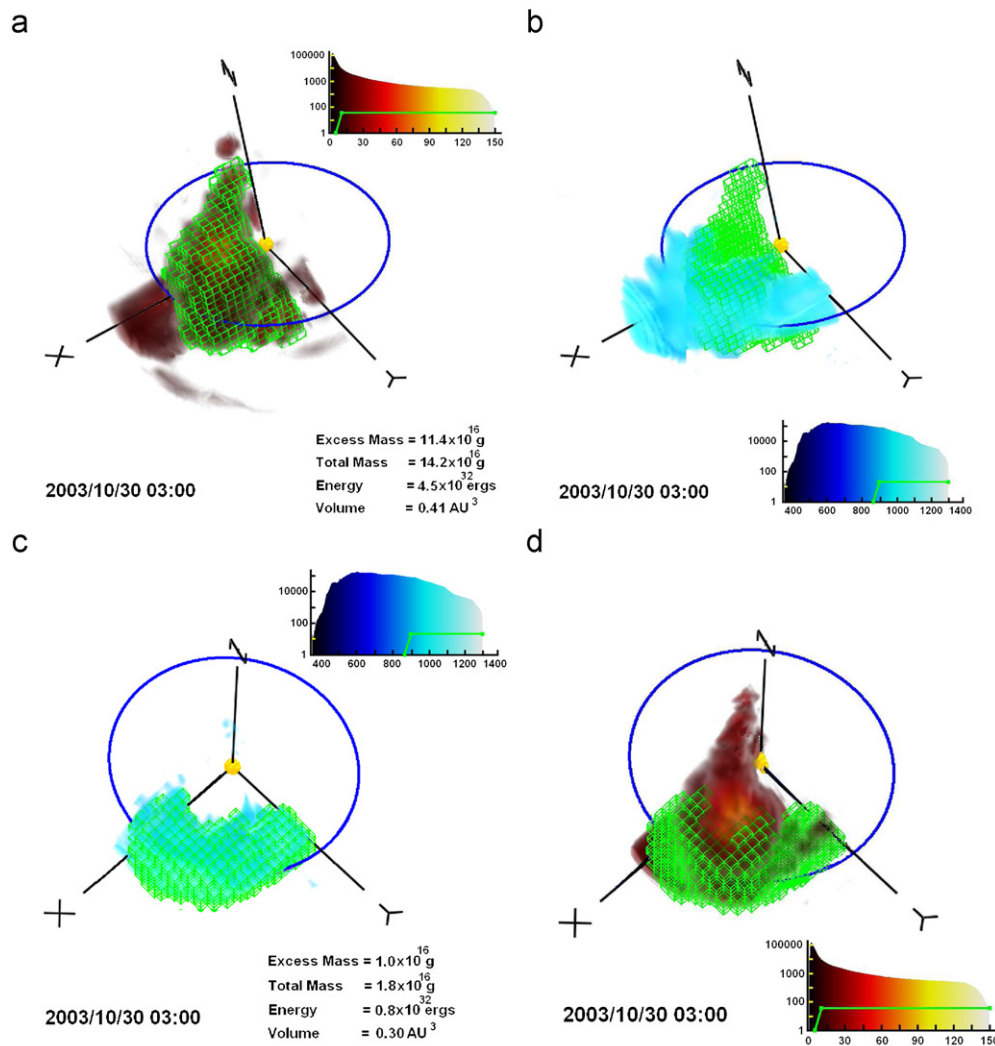


**Fig. 7.** 3-D reconstruction of the heliospheric response to the 28 October 2003 CME using SMEI Thomson-scattering and IPS velocity data. (a) The SMEI CME density structure above  $10 \text{ e}^- \text{ cm}^{-3}$  is highlighted by cubes. Each cube is mapped to the IPS velocity volume (b) to determine the velocities associated with the dense CME structure. For each cube (i) highlighted, an energy determination is made by multiplying the total mass within the cube. Summed over the total highlighted material ( $\sum(1/2)m_i v_i^2$ ) this provides the total energy of the outward flowing dense structure. (c) The 3-D SMEI density reconstruction in this volume has had each cube mapped from (d) the CME velocity structure above  $900 \text{ km s}^{-1}$  highlighted by cubes. Summed over the total highlighted material this provides the energy associated with the outward-flowing high velocity CME structure.

et al., 2007a), and at the Ulysses Spacecraft (e.g., Fujiki et al., 2003; Hayashi et al., 2003b; Kojima et al., 2007; Bisi et al., 2007b, 2008b, 2010a), and finally using a variety of data sets from radio arrays in Cambridge (UK), STELab, the Ootacamund (Ooty) Radio Telescope (ORT), in India, and the European Incoherent SCATter (EISCAT) radar telescopes in northern Scandinavia. For Thomson-scattering data sets, comparisons of 3-D reconstructions from Helios photometer data have been made with in-situ data from the Helios spacecraft (Jackson et al., 2001; Jackson and Hick, 2005), and reconstructions from SMEI compared with many different near-Earth monitors and STEREO in-situ measurements (e.g., Jackson et al., 2008a, 2010a, under review; Bisi et al., 2008a). These comparisons become more successful as the numbers of lines of sight available from the remote-sensing data sets increase, and thus enhance the 3-D reconstruction resolution.

## 5. Conclusions

3-D reconstruction of heliospheric structure has a long history, but it has relied heavily on the availability of suitable

data. Remote sensing of heliospheric structure began in earnest with the IPS observations from the 81 MHz Cambridge (UK) radio array telescope that began operation in the late 1950s (Hewish et al., 1964). Observations from this array, from 1990 through 1994, included nearly 1000 useful radio sources daily. In the early 1970s analyses using data from a three-site system near San Diego, California (USA) began operating at 73 MHz to measure IPS velocities from more than ten sources daily. Useful data from this system provided reconstructed heliospheric velocities, and extended into the middle of the 1980s. The STELab (Japan) IPS radio array system at 327 MHz began full operation to measure three-site velocities in early 1985, and observations have continued to the present extending from spring until winter in Japan. In more recent years (from about the year 2000) this system has provided scintillation-level observations (that provide a proxy for density) for several tens of sources daily. A new radio array that has been constructed and is now operating near Toyokawa in Japan is expected to deliver considerably improved performance and provide intensity-scintillation spectra for  $>100$  radio sources per day along with year-around operation (Kojima et al., 2002).

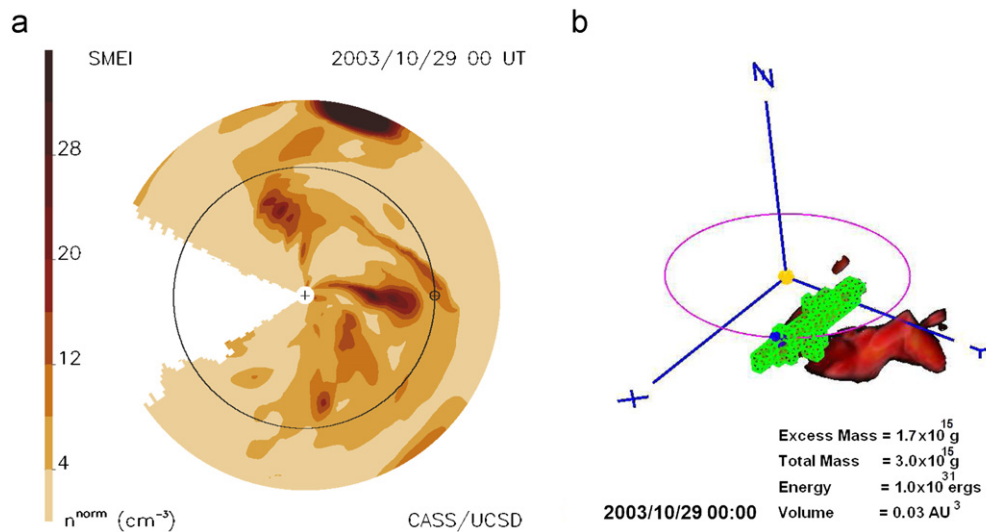


**Fig. 8.** A CME density enhancement viewed in front of the 28 October 2003 CME at the approximate location of the shock sheath. (a) In the ecliptic cut shown the Sun is centered and the Earth is to the right on its circular orbit. As in previous volumetric analyses, an  $r^{-2}$  density fall-off normalized to 1 AU has been removed from the volume to better show structures at different radial distances from the Sun. A large density enhancement associated with the 28 October 2003 CME is shown moving outward approximately along the Sun–Earth line following the initial response that passed at the beginning of 29 October. A density structure at the front of the high velocity structure mapped in Fig. 7 precedes it into space. An area of the volume that cannot be reconstructed in the SMEI analysis is present opposite the Sun from the Earth, and is left blank. (b) The high density in front of the high speed region is shown as a remote observer would view it. The density structure is highlighted by cubes and its mass and volume estimated. Note that the structure does not form a continuous dense front ahead of the high velocity.

Other IPS systems from different locations around the world have contributed data to this 3-D reconstruction technique. These include velocity and density 3-D reconstructions using data from Ooty (Bisi et al., 2008b, 2009b), and velocity 3-D reconstructions using data from EISCAT (Bisi et al., 2007a, 2010a). Future instruments that could join in this effort include the MEXican Array Radio Telescope (MEXART) array now operating near Michoacan (Mexico), the Murchison Widefield Array (MWA) now under construction and initial testing in Western Australia, and the LOw Frequency ARray (LOFAR) in The Netherlands and throughout several other European countries including Germany and the UK.

Initially, the Helios photometer data proved that global Thomson-scattering observations are feasible by demonstrating that a long-term base can be subtracted (Jackson and Hick, 2005, and references therein) which isolates the Thomson-scattering contribution. These analyses next led to the design and the near-Earth flight SMEI whose data enabled higher-resolution 3-D reconstruction of global heliospheric structure from this nearby vantage point. SMEI's precision photometry, near-all-sky coverage, and high telemetry rate represent a nearly 1000-fold improvement over the data from Helios. These have in turn enabled 3-D reconstructions which have been applied to viewing and analyzing both transient and co-rotating heliospheric density structures from 2003 to the present. Even higher resolutions for density 3-D reconstructions are possible using SMEI observations; the current limit has been set by computer resources that have limited the numbers of lines of sight utilized to  $\sim 2\%$  of those available. Utilizing all lines of sight in the SMEI Thomson-scattering analyses can theoretically increase resolutions in space and time many-fold.

Current perspective analyses using data from the NASA's twin STEREO spacecraft (Kaiser et al., 2008) have focused coronal and heliospheric studies on ways to provide 3-D analyses of coronal and inner-heliospheric structures. These analyses often employ remote-sensing data only from the STEREO SECCHI instrument suite (Howard et al., 2008). From as long ago as Katz (1978) it was shown that depending on the choice of orientation and resolution of the 3-D matrix shape relative to the images, even a single perspective view can provide a unique solution for an object's 3-D

structure. Many of the techniques used to determine coronal structure in three dimensions are reviewed recently by Mierla et al. (2010), and some of these have been applied to structures observed by the STEREO Heliospheric Imager (HI) instrumentation (Eyles et al., 2009). It is indeed possible to accurately identify very fine features in two views and extrapolate the motion of these outward into the heliosphere. However, an extension of this technique to include the whole detailed 3-D coronal structure that maps to different brightness at the resolutions of the individual images is not possible, simply because two perspective-views do not contain enough information to accomplish this. On the other hand, it is also clear that heliospheric structures that are smooth topologically can be located unambiguously in three dimensions, but with less accuracy than the original image resolutions, since even a direction measurement of the structure from a single view allows some 3-D location information about the structure.

We note that many others currently use techniques similar to Jackson et al. (1985), Behannon et al. (1991), or Tokumaru et al. (2003a,b) to locate structures such as CMEs that have been viewed by STEREO, by coronagraphs, or by SMEI using difference-image observations alone (e.g., Lugaz et al., 2008; Wood et al., 2009; Tappin and Howard, 2009). We do not review these analyses techniques here, but note that most of these methods, of necessity, employ CME templates derived from bulk-density models comparing these to difference-images. Using difference images in the comparison has the advantage that most longer-term background contaminations are removed, but with the major disadvantage that a large portion of the Thomson-scattered signal is also removed in the process. As a result, CME features that change more slowly (hours to days) than the shorter time between the differences are also subtracted away. There is an inherent difficulty in this since the true LOS brightness of the response from the bulk density of the CME model should be fit to measurements where only a very long-term (many day) base is removed. As shown in Jackson et al. (2009), difference images tend to highlight the steep gradients usually at the fronts of CMEs, and are thus not representative of the bulk density that is encompassed by the models. Not only does this make bulk density interpretation difficult, but most likely it places

the fitted CME structure at the wrong location along the line of sight.

The UCSD IPS heliospheric 3-D reconstruction inversion tomography was one of the first programs presented to the Community Coordinated Modeling Center (CCMC) at the Goddard Space Flight Center circa the year 2000. This IPS time-dependent 3-D reconstruction program was recently (2010) updated to provide higher-resolution velocity and density 3-D reconstructions from existing IPS data sets. In addition, the 3-D technique that provides density reconstructions from SMEI data at even higher temporal and spatial resolutions is now also extant at the CCMC. With continued operation of IPS arrays, SMEI, and the STEREO SECCHI remote-sensing imagers, we expect even more use for these analyses. Similar remote-sensing observations are planned for the upcoming Solar Orbiter Mission, and for the recently announced NASA Heliospheric Mission, Solar Probe Plus. Thus, we expect that these tomographic analyses will find even more use in coming years.

## Acknowledgments

The IPS analysis and these 3-D reconstruction techniques were enhanced significantly by a joint STELab – Center for Astrophysics and Space Sciences, UCSD cooperative agreement begun in 1997 and continuing through to the present. This has allowed an exchange of students, professors, and researchers between the two institutions, to study and analyze both IPS and SMEI data. SMEI was designed and constructed by a team of scientists and engineers from the US Air Force Research Laboratory, the University of California, San Diego, Boston College, Boston University, and the University of Birmingham, UK. The work of UCSD-based authors was supported at UCSD by NSF Grants ATM-0852246 and ATM0925023, and also by NASA Grant NNX08AJ11G. M.M. Bisi has also more recently been supported by funding on a rolling grant to Aberystwyth University in Wales (UK) from the Science and Technology Facilities Council (STFC) in the UK.

## References

- Anderson, D.L., Dziewonski, A.M., 1984. Seismic tomography. *Sci. Am.* 251 (4), 60–68.
- Anderson Jr., D.E., Meier, R.R., Hodges Jr., R.R., Tinsley, B.A., 1987. Hydrogen Balmer alpha intensity distribution and line profiles from multiple scattering theory using realistic geocoronal models. *J. Geophys. Res.* 92, 7619–7642.
- Anzer, U., 1978. Can coronal loop transients be driven magnetically? *Sol. Phys.* 57, 111–118.
- Asai, K., Kojima, M., Tokumaru, M., Yokobe, A., Jackson, B.V., Hick, P.L., Manoharan, P.K., 1998. Heliospheric tomography using interplanetary scintillation observations 3. Correlation between speed and electron density fluctuations in the solar wind. *J. Geophys. Res.* 103, 1991–2001.
- Behannon, K.W., Burlaga, L.F., Hewish, A., 1991. Structure and evolution of compound streams at  $\leq 1$  AU. *J. Geophys. Res.* 96, 21,213–21,225.
- Billings, D.E., 1966. *A Guide to the Solar Corona*. Academic Press, New York.
- Bisi, M.M., Jackson, B.V., Fallows, R.A., Breen, A.R., Hick, P.P., Wannberg, G., Thomasson, P., Jordan, C.A., Dorrian, G.D., 2007a. Combined STELab, EISCAT, ESR, and MERLIN IPS observations of the solar wind. *Proc. SPIE* 6689, 1–10.
- Bisi, M.M., Jackson, B.V., Hick, P.P., Buffington, A., Clover, J.M., 2007b. Coronal mass ejection reconstructions from interplanetary scintillation data using a kinematic model: a brief review. *Adv. Geosci.* 14, 161–181.
- Bisi, M.M., Jackson, B.V., Hick, P.P., Buffington, A., Odstrcil, D., Clover, J.M., 2008a. 3D reconstructions of the early November 2004 CDAW geomagnetic storms: preliminary analysis of STELab IPS speed and SMEI density. *J. Geophys. Res.* 113, A00A11. doi:10.1029/2008JA013222.
- Bisi, M.M., Jackson, B.V., Buffington, A., Hick, P.P., Manoharan, P.K., Clover, J.M., 2008b. Solar wind and CME studies of the inner heliosphere using IPS data from ORT and EISCAT. *Adv. Geosci.* 21, 1–17.
- Bisi, M.M., Jackson, B.V., Buffington, A., Clover, J.M., Hick, P.P., Tokumaru, M., 2009a. Low-resolution STELab IPS 3D reconstructions of the whole heliospheric interval and comparison with in-ecliptic solar wind measurements from STEREO and Wind instrumentation. *Sol. Phys.* 256, 201. doi:10.1007/s11207-009-9350-9.
- Bisi, M.M., Jackson, B.V., Clover, J.M., Manoharan, P.K., Tokumaru, M., Hick, P.P., Buffington, A., 2009b. 3D reconstructions of the early-November 2004 CDAW geomagnetic storms: analysis of Ooty IPS speed and density data. *Ann. Geophys.* 27, 4479–4489.
- Bisi, M.M., Jackson, B.V., Breen, A.R., Dorrian, G.D., Fallows, R.A., Clover, J.M., Hick, P.P., 2010a. Three-dimensional (3-D) reconstructions of EISCAT IPS velocity data in the declining phase of solar cycle 23. *Sol. Phys.* 265, 233–244.
- Bisi, M.M., Breen, A.R., Jackson, B.V., Fallows, R.A., Walsh, A.P., Mikić, Z., Riley, P., Owen, C.J., Gonzalez-Esparza, A., Aguilar-Rodriguez, E., Morgan, H., Jensen, E.A., Wood, A.G., Owens, M.J., Tokumaru, M., Manoharan, P.K., Chashei, I.V., Giunta, A., Linker, J.A., Shishov, V.I., Tyul'bashev, S.A., Agalya, G., Glubokova, S.K., Hamilton, M.S., Fujiki, K., Hick, P.P., Clover, J.M., Pintér, B., 2010b. From the Sun to the Earth: the 13 May 2005 coronal mass ejection. *Sol. Phys.* 265, 49–127.
- Bracewell, R.N., 1956. Strip integration in radio astronomy. *Aust. J. Phys.* 9, 198–217.
- Brueckner, G.E., Howard, R.A., Koomen, M.J., Korendyke, C.M., Michels, D.J., Moses, J.D., Socker, D.G., Dere, K.P., Lamy, P.L., Llebaria, A., Bout, M.V., Schwenn, R., Simnett, G.M., Bedford, D.K., Eyles, C.J., 1995. The large angle spectroscopic coronagraph (LASCO): visible light coronal imaging and spectroscopy. *Sol. Phys.* 162, 357–402.
- Burlaga, L., Lepping, R., Weber, R., Armstrong, T., Goodrich, C., Sullivan, J., Gurnett, D., Kellogg, P., Keppler, E., Mariani, F., Neubauer, F., Rosenbauer, H., Schwenn, R., 1980. Interplanetary particles and fields, November 22–December 7, 1977: Helios, Voyager, and IMP observations between 0.6 AU and 1.6 AU. *J. Geophys. Res.* 85, 2227–2242.
- Butala, M.D., Hewett, R.J., Frazin, R.A., Kamalabadi, F., 2010. Dynamic three-dimensional tomography of the solar corona. *Sol. Phys.* 262, 495–509.
- Chapman, R.W., 1979. NASA's search for the solar connection-II. *Sky Telescope* 58 (3), 223–227.
- Coles, W.A., Kaufman, J.J., 1978. Solar wind velocity estimation from multi-station IPS. *Radio Sci.* 13, 591–597.
- Coles, W.A., Rickett, B.J., Rumsey, V.H., Kaufman, J.J., Turley, D.G., Ananthakrishnan, S., Armstrong, J.W., Harmon, J.K., Scott, S.L., Sime, D.G., 1980. Solar cycle changes in the polar solar wind. *Nature* 286, 239–241.
- Crifo, F., Picat, J.P., Cailloux, M., 1983. Coronal transients: loop or bubble? *Sol. Phys.* 83, 143–152.
- Domingo, V., Fleck, B., Poland, A.I., 1995. SOHO: the solar and heliospheric observatory. *Space Sci. Rev.* 72, 81–84.
- Dunn, T., Jackson, B.V., Hick, P.P., Buffington, A., Zhao, X.P., 2005. Comparative analyses of the CSSS calculation in the UCSD tomographic solar observations. *Sol. Phys.* 227, 339–353.
- Eyles, C.J., Simnett, G.M., Cooke, M.P., Jackson, B.V., Buffington, A., Hick, P.P., Waltham, N.R., King, J.M., Anderson, P.A., Holladay, P.E., 2003. The solar mass ejection imager (SMEI). *Sol. Phys.* 217, 319–347.
- Eyles, C.J., Harrison, R.A., Davis, C.J., Waltham, N.R., Shaughnessy, B.M., Mapson-Menard, H.C.A., Bewsher, D., Crothers, S.R., Davies, J.A., Simnett, G.M., Howard, R.A., Moses, J.D., Newmark, J.S., Socker, D.G., Halain, J.P., Defise, J.M., Mazy, E., Rochus, P., 2009. The heliospheric imagers on-board the STEREO mission. *Sol. Phys.* 254, 387. doi:10.1007/s11207-008-9299-0.
- Frazin, R.A., 2000. Tomography of the solar corona. I. A robust, regularized, positive estimation method. *Astrophys. J.* 530, 1026–1035.
- Frazin, R.A., Janzen, P., 2002. Tomography of the solar corona. II. Robust, regularized, positive estimation of the three-dimensional electron density distribution from LASCO-C2 polarized white-light images. *Astrophys. J.* 570, 408–422.
- Frey, S., Frey, H.U., Carr, D.J., Bauer, O.H., Haerendel, G., 1996. Auroral emission profiles extracted from three-dimensionally reconstructed arcs. *J. Geophys. Res.* 101, 21,731–21,741.
- Fujiki, K., Kojima, M., Tokumaru, M., Ohmi, T., Yokobe, A., Hayashi, K., McComas, D.J., Elliott, H.A., 2003. How did the solar wind structure change around the solar maximum?—From interplanetary scintillation observation. *Ann. Geophys.* 21, 1257–1261.
- Galvin, A.B., Kistler, L.M., Popecki, M.A., Farrugia, C.J., Simunac, K.D.C., Ellis, L., Möbius, E., Lee, M.A., Boehm, M., Carroll, J., Crawshaw, A., Conti, M., Demaine, P., Ellis, S., Gaidos, J.A., Googins, J., Granoff, M., Gustafson, A., Heirtzler, D., King, B., Knauss, U., Levasseur, J., Longworth, S., Singer, K., Turco, S., Vachon, P., Vosbury, M., Widholm, M., Blush, L.M., Karrer, R., Bochsler, P., Daoudi, H., Etter, A., Fischer, J., Jost, J., Opitz, A., Sigrist, M., Wurz, P., Klecker, B., Ertl, M., Seidenschwang, E., Wimmer-Schweingruber, R.F., Koeten, M., Thompson, B., Steinfeld, D., 2008. The plasma and suprathermal ion composition (PLASTIC) investigation on the STEREO observatories. *Space Sci. Rev.* 136, 437–486. doi:10.1007/s11214-007-9296-x.
- Gapper, G.R., Hewish, A., Purvis, A., Duffett-Smith, P.J., 1982. Observing interplanetary disturbances from the ground. *Nature* 296, 633–636.
- Garcia, F.J., Taylor, M.J., Kelley, M.C., 1997. Two-dimensional spectral analysis of mesospheric airglow image data. *Appl. Opt.* 36, 7374–7385.
- Gies, D., Fullerton, A.W., Boulton, C.T., Bagnuolo Jr., W.G., Hahula, M.E., Wiemker, R., 1994. HD 53975: an O-type spectroscopic binary with a large mass ratio. *Astrophys. J.* 422, 823–830.
- Gilbert, P., 1972. Iterative methods for the three-dimensional reconstruction of an object from projections. *J. Theor. Biol.* 36, 105–117.
- Gorunov, M.E., 1996. Three-dimensional satellite refractive tomography of the atmosphere: numerical simulation. *Radio Sci.* 31 (1), 95–104.
- Harrison, R.A., Davies, J.A., Rouillard, A.P., Davis, C.J., Eyles, C.J., Bewsher, D., Crothers, S.R., Howard, R.A., Sheeley, N.R., Vourlidis, A., Webb, D., Brown, D.S., Dorrian, G., 2009. Two years of the STEREO heliospheric imagers. *Sol. Phys.* 256, 219–237.
- Hayashi, K., Fujiki, K., Kojima, M., Tokumaru, M., 2003a. Basic results of MHD tomography analysis method for IPS observations. In: Velli, M., Bruno, R., Malara, F. (Eds.), *Proceedings of Solar Wind X*, 679. AIP Conference Proceedings, pp. 144–147.

- Hayashi, K., Kojima, M., Tokumaru, M., Fujiki, K., 2003b. MHD tomography using interplanetary scintillation measurement. *J. Geophys. Res.* 108, 1102. doi:10.1029/2002JA009567.
- Hewish, A., Bravo, S., 1986. The sources of large-scale heliospheric disturbances. *Sol. Phys.* 106, 185–200.
- Hewish, A., Scott, P.F., Wills, D., 1964. Interplanetary scintillation of small diameter radio sources. *Nature* 203, 1214–1217.
- Hick, P.P., Jackson, B.V., 2004. Heliospheric tomography: an algorithm for the reconstruction of the 3D solar wind from remote sensing observations. In: Fineschi, S., Gumm, M.A. (Eds.), *Telescopes and Instrumentation for Solar Astrophysics*, 5171. Proceedings of SPIE, pp. 287–297.
- Hick, P., Jackson, B.V., Rappoport, S., Woan, G., Slater, G., Strong, K., Uchida, Y., 1995. Synoptic IPS and Yohkoh soft X-ray observations. *Geophys. Res. Lett.* 22, 643–646.
- Hoeksema, J.T., Wilcox, J.M., Scherrer, P.H., 1983. The structure of the heliospheric current sheet. *J. Geophys. Res.* 88, 9910–9918.
- Houminer, Z., 1971. Corotating plasma streams revealed by interplanetary scintillations. *Nat. Phys. Sci.* 231, 165–167.
- Houminer, Z., Gallager, F., 1993. A search for coronal streamers near 1 AU using interplanetary scintillation. *Sol. Phys.* 145, 359–375.
- Howard, R.A., Moses, J.D., Vourlidis, A., Newmark, J.S., Socker, D.G., Plunkett, S.P., et al., 2008. Sun earth connection coronal and heliospheric investigation (SECCHI). *Space Sci. Rev.* 136, 67–115.
- Hurlburt, E., Martens, C.H., Slater, G., Jaffey, S.M., 1994. Volume reconstruction of magnet fields using solar imagery. In: Balasubramaniam, K.S., Simon, G.W. (Eds.), *Solar Active Region Evolution: Comparing Models with Observations*, ASP Conference Series, vol. 68, pp. 30–36.
- Jackson, B.V., 1977. A coronal hole equatorial extension and its relation to a high speed solar wind stream. In: *A Topical Conference on Solar and Interplanetary Physics*, Tucson, Arizona, January 12–15, pp. 7–9.
- Jackson, B.V., 1985a. Helios observations of the earthward-directed mass ejection of 27 November, 1979. *Sol. Phys.* 95, 363–370.
- Jackson, B.V., 1985b. Imaging of coronal mass ejections by the Helios spacecraft. *Sol. Phys.* 100, 563–574.
- Jackson, B.V., 1986. Remote sensing observations of mass ejections and shocks in interplanetary space. *Adv. Space Res.* 6, 307–310.
- Jackson, B.V., 1991. Helios spacecraft photometer observations of elongated corotating structures in the interplanetary medium. *J. Geophys. Res.* 96, 11,307–11,318.
- Jackson, B.V., Leinert, C., 1985. Helios images of solar mass ejections. *J. Geophys. Res.* 90, 10,759–10,764.
- Jackson, B.V., Hick, P.L., 1994. Three dimensional reconstruction of coronal mass ejections. In: *Proceedings of the Third SOHO Workshop, Solar Dynamic Phenomena and Solar Wind Consequences*, ESA SP-373, pp. 199–202.
- Jackson, B.V., Froehling, H.R., 1995. Three-dimensional reconstruction of coronal mass ejections. *Astron. Astrophys.* 299, 885–892.
- Jackson, B.V., Hick, P., 2000. Three dimensional tomography of heliospheric features using global Thomson scattering data. *Adv. Space Res.* 25 (9), 1875–1878.
- Jackson, B.V., Hick, P.P., 2002. Corotational tomography of heliospheric features using global Thomson scattering data. *Sol. Phys.* 211, 344–356.
- Jackson, B.V., Hick, P.P., 2005. Three-dimensional tomography of interplanetary disturbances. In: Gary, D.E., Keller, C.U. (Eds.), *Solar and Space Weather Radiophysics, Current Status and Future Developments*, Astrophysics and Space Science Library, vol. 314. Kluwer Academic Publishers, Dordrecht, The Netherlands, pp. 355–386 Chapter 17.
- Jackson, B.V., Howard, R.A., Sheeley Jr., N.R., Michels, D.J., Koomen, M.J., Illing, R.M.E., 1985. Helios spacecraft and earth perspective observations of three looplike solar mass ejections. *J. Geophys. Res.* 90, 5075–5081.
- Jackson, B.V., Rimpolt, B., Svestka, Z., 1988. Solar and interplanetary observations of the mass ejection on 7 May, 1979. *Sol. Phys.* 115, 327–343.
- Jackson, B.V., Hick, P.L., Kojima, M., Yokobe, A., 1997b. Heliospheric tomography using interplanetary scintillation observations. *Adv. Space Res.* 20 (1), 23–26.
- Jackson, B.V., Hick, P.L., Kojima, M., Yokobe, A., 1998. Heliospheric tomography using interplanetary scintillation observations 1. Combined Nagoya and Cambridge data. *J. Geophys. Res.* 103, 12,049–12,067.
- Jackson, B.V., Buffington, A., Hick, P.P., 2001. A heliospheric imager for Solar Orbiter. In: *Proceedings of Solar Encounter: The First Solar Orbiter Workshop*, ESA SP-493, May 14–18, 2001, Santa Cruz de Tenerife, Spain, pp. 251–254.
- Jackson, B.V., Hick, P.P., Buffington, A., Kojima, M., Tokumaru, M., Fujiki, K., Ohmi, T., Yamashita, M., 2003. Time-dependent tomography of heliospheric features using interplanetary scintillation (IPS) remote-sensing observations. In: Velli, M., Bruno, R., Malara, F. (Eds.), *Proceedings of Solar Wind X*, AIP Conference Proceedings, vol. 679, pp. 75–78.
- Jackson, B.V., Buffington, A., Hick, P.P., Altrick, R.C., Figueroa, S., Holladay, P.E., Johnston, J.C., Kahler, S.W., Mozer, J.B., Price, S., Radick, R.R., Sagalyn, R., Sinclair, D., Simnett, G.M., Eyles, C.J., Cooke, M.P., Tappin, S.J., Kuchar, T., Mizuno, D., Webb, D.F., Anderson, P.A., Keil, S.L., Gold, R.E., Waltham, N.R., 2004. The solar mass ejection imager (SMEI) mission. *Sol. Phys.* 225, 177–207.
- Jackson, B.V., Buffington, A., Hick, P.P., Wang, X., Webb, D., 2006. Preliminary three-dimensional analysis of the heliospheric response to the 28 October 2003 CME using SMEI white-light observations. *J. Geophys. Res.* 111 (A4), A04S91.
- Jackson, B.V., Boyer, J.A., Hick, P.P., Buffington, A., Bisi, M.M., Crider, D.H., 2007a. Analysis of solar wind events using interplanetary scintillation (IPS) remote sensing 3D reconstructions and their comparison at Mars. *Sol. Phys.* 241 (2), 385–396. doi:10.1007/s11207-007-0276-9.
- Jackson, B.V., Hick, P.P., Buffington, A., Bisi, M.M., Jensen, E.A., 2007b. SMEI observations in the STEREO era. *Proceedings of SPIE* 6689 (6689OG), 1–14. doi:10.1117/12.734870.
- Jackson, B.V., Bisi, M.M., Hick, P.P., Buffington, A., Clover, J.M., Sun, W., 2008a. Solar Mass Ejection Imager (SMEI) 3D reconstruction of the 27–28 May 2003 CME sequence. *J. Geophys. Res.* 113, A00A15. doi:10.1029/2008JA013224.
- Jackson, B.V., Hick, P.P., Buffington, A., Bisi, M.M., Clover, J.M., Tokumaru, M., 2008b. Solar Mass Ejection Imager (SMEI) and interplanetary scintillation (IPS) 3D-reconstructions of the inner heliosphere. *Adv. Geosci.* 21, 339–366.
- Jackson, B.V., Hick, P.P., Buffington, A., Bisi, M.M., Clover, J.M., 2009. SMEI direct, 3D-reconstruction sky maps, and volumetric analyses, and their comparison with SOHO and STEREO observations. *Ann. Geophys.* 27, 4097–4104.
- Jackson, B.V., Hick, P.P., Buffington, A., Bisi, M.M., Clover, J.M., Tokumaru, M., Fujiki, K., 2010a. 3D reconstruction of density enhancements behind interplanetary shocks from Solar Mass Ejection Imager white-light observations. In: Maksimovic, M., Issautier, K., Meyer-Vernet, N., Moncuquet, M., Pantellini, F. (Eds.), *Proceedings of Solar Wind 12*, AIP Conference Proceedings, vol. 1216, pp. 659–662.
- Jackson, B.V., Hick, P.P., Bisi, M.M., Clover, J.M., Buffington, A., 2010b. Inclusion of in-situ velocity measurements into the UCSD time-dependent tomography to constrain and better-forecast remote-sensing observations. *Sol. Phys.* 265, 245–256. doi:10.1007/s11207-010-9529-0.
- Jackson, B.V., Buffington, A., Hick, P.P., Bisi, M.M., Clover, J.M., 2010c. A heliospheric imager for deep space: lessons learned from Helios, SMEI, and STEREO. *Sol. Phys.* 265, 257–275. doi:10.1007/s11207-010-9579-3.
- Jackson, B.V., Hamilton, M.S., Hick, P.P., Buffington, A., Bisi, M.M., Clover, J.M., Tokumaru, M., Fujiki, K., Solar Mass Ejection Imager (SMEI) 3-D reconstruction of density enhancements behind interplanetary shocks: in-situ comparison near Earth and at STEREO. *J. Atmos. Sol. Terr. Phys.*, under review.
- James, J.F., Mukai, T., Watanabe, T., Ishiguro, M., Nakamura, R., 1997. The morphology and brightness of the zodiacal light and Gegenschein. *Mon. Not. R. Astron. Soc.* 288, 1022–1026.
- Kaiser, M.L., Kucera, T.A., Davila, J.M., St. Cyr, O.C., Guhathakurta, M., Christian, E., 2008. The STEREO mission. In: Russell, C. (Ed.), *Space Sci. Rev.* 136, 5.
- Kakinuma, T., 1977. Observations of interplanetary scintillation: solar wind velocity measurements. In: Shea, M.A., Smart, D.F., Wu, S.T. (Eds.), *Study of Traveling Interplanetary Phenomena*. D. Reidel, Norwell, Mass, pp. 101–118.
- Katz, M.B., 1978. Questions of uniqueness and resolution in reconstruction from projections. In: Levin, S. (Ed.), *Lecture Notes in Biomathematics*, vol. 26. Springer-Verlag, New York.
- Kojima, M., Kakinuma, T., 1987. Solar cycle evolution of solar wind speed structure between 1973 and 1985 observed with the interplanetary scintillation method. *J. Geophys. Res.* 92, 7269–7279.
- Kojima, M., Kakinuma, T., 1990. Solar cycle dependence of global distribution of solar wind speed. *Space Sci. Rev.* 53, 173–222.
- Kojima, M., Watanabe, H., Yamauchi, Y., Misawa, H., 1996. Acceleration phenomena of high speed wind observed at 0.1–0.3 AU with interplanetary scintillation. In: Winterhalter, D., Gosling, J.T., Habbal, S.R., Kurth, W.S., Neugebauer, M. (Eds.), *Solar Wind Eighth AIP Conference Proceedings*, vol. 382. Woodbury, New York, pp. 109–112.
- Kojima, M., Asai, K., Hick, P.L., Jackson, B.V., Tokumaru, M., Watanabe, H., Yokobe, A., 1997. Solar wind structure at 0.1–1 AU reconstructed from IPS observations using tomography. In: Habbal, S.R. (Ed.), *Robotic Exploration Close to the Sun: Scientific Basis*. AIP Conference Proceedings 385, pp. 97–104.
- Kojima, M., Tokumaru, M., Watanabe, H., Yokobe, A., Asai, K., Jackson, B.V., Hick, P.L., 1998. Heliospheric tomography using interplanetary scintillation observations, 2. Latitude and heliocentric distance dependence of solar wind structure at 0.1–1 AU. *J. Geophys. Res.* 103, 1981–1989.
- Kojima, M., Fujiki, K., Ohmi, T., Tokumaru, M., Yokobe, A., Hakamada, K., 2001. Latitudinal velocity structures up to the solar poles estimated from interplanetary scintillation tomography analysis. *J. Geophys. Res.* 106, 15,677–15,686.
- Kojima, M., Tokumaru, M., Fujiki, K., Ishida, Y., Ohmi, T., Hayashi, K., Yamashita, M., 2002. Solar wind imaging facility (SWIFT) for space weather research. In: *Proceedings of SPIE, Waikoloa*, 22–28 August 2002, 4853, 121, doi:10.1117/12.460271.
- Kojima, M., Fujiki, K., Hirano, M., Tokumaru, M., Ohmi, T., Hakamada, K., 2004. Solar wind properties from IPS observations. In: Poletto, G., Suess, S.T. (Eds.), *The Sun and the Heliosphere as an Integrated System*. Kluwer Academic Publishers, pp. 147–178.
- Kojima, M., Tokumaru, M., Fujiki, K., Hayashi, K., Jackson, B.V., 2007. IPS tomographic observations of 3D solar wind structure. In: Chashei, I., Shishov, V. (Eds.), *Scattering and Scintillation in Radio Astronomy*, *Astronomical and Astrophysical Transactions*, 26:6, pp. 467–476, doi:10.1080/10556790701596200.
- Leinert, C., Klüppelberg, D., 1974. Stray light suppression in optical space experiments. *Appl. Opt.* 13, 556–564.
- Leinert, C., Pitz, E., 1989. Zodiacal light observed by Helios through solar cycle No. 21. *Astron. Astrophys.* 210, 399–402.
- Leinert, C., Pitz, E., Link, H., Salm, N., 1981a. Calibration and inflight performance of the zodiacal light experiment on Helios. *J. Space Sci. Instrum.* 5, 257–261.
- Leinert, C., Link, H., Pitz, E., Salm, N., Knuettelberg, D., 1975. Helios zodiacal light experiment. *Raumfahrtforschung* 19, 264–267.
- Leinert, C., Richter, I., Pitz, E., Planck, B., 1981b. The zodiacal light from 1.0 to 0.3 AU as observed by the HELIOS space probes. *Astron. Astrophys.* 103 (1), 177–188.
- Leinert, C., Richter, I., Planck, B., 1982. Stability of the zodiacal light from minimum to maximum of the solar cycle (1974–1981). *Astron. Astrophys.* 110, 111–114.

- Lugaz, N., Vourlidas, A., Roussev, I.I., Jacobs, C., Manchester IV, W.B., Cohen, O., 2008. The brightness of density structures at large solar elongation angles: what is being observed by STEREO SECCHI? *Astrophys. J.* 684 L111. doi:10.1086/592217.
- MacQueen, R.M., 1993. The three-dimensional structure of 'loop-like' coronal mass ejections. *Sol. Phys.* 145, 169–188.
- Marsh, T.R., Horne, K., 1988. Images of accretion disks—II Doppler tomography. *Mon. Not. R. Astron. Soc.* 235, 269–286.
- McComas, D.J., Phillips, J.L., Bame, S.J., Gosling, J.T., Goldstein, B.E., Neugebauer, M., 1995. Ulysses solar wind observations to 56 deg south. *Space Sci. Rev.* 72, 93–99.
- Meier, R.R., Mange, P., 1973. Spatial and temporal variations of the Lyman-alpha airglow and related atomic hydrogen distributions. *Planet. Space Sci.* 21 (3), 309–327.
- Mierla, M., Inhester, B., Antunes, A., Boursier, Y., Byrne, J.P., Colaninno, R., Davila, J., de Koning, C.A., Gallagher, P.T., Gissot, S., Howard, R.A., Howard, T.A., Kramar, M., Lamy, P., Liewer, P.C., Maloney, S., Marqué, C., McAteer, R.T.J., Moran, T., Rodriguez, L., Srivastava, N., St. Cyr, O.C., Stenborg, G., Temmer, M., Thernisien, A., Vourlidas, A., West, M.J., Wood, B.E., Zhukov, A.N., 2010. On the 3D reconstruction of coronal mass ejections using coronagraph data. *Ann. Geophys.* 28, 203–215. doi:10.5194/angeo-28-203-2010.
- Mizuno, D.R., Buffington, A., Cooke, M.P., Eyles, C.J., Hick, P.P., Holladay, P.E., Jackson, B.V., Johnston, J.C., Kuchar, T.A., Mozer, J.M., Price, S.D., Radick, R.R., Simnett, G.M., Sinclair, D., Webb, D.F., 2005. Very high-altitude aurora observations with the Solar Mass Ejection Imager. *J. Geophys. Res.* 110, A07230. doi:10.1029/2004JA010689.
- Moran, T.G., Davila, J.M., 2004. Three-dimensional polarimetric imaging of coronal mass ejections. *Science* 305, 66–70. doi:10.1126/science.1098937.
- Mouschovias, T., Poland, A.I., 1978. Expansion and broadening of coronal loop transients: a theoretical explanation. *Astrophys. J.* 220, 675–682.
- Munro, R.H., 1977. Coronal transients: arches or bubbles? In: *Topical Conference on Solar and Interplanetary Physics*, January 12–15, Tucson, Arizona, pp. 10.
- Panasnyuk, A.V., 1999. Three-dimensional reconstruction of UV emissivities in the solar corona using ultraviolet coronagraph spectrometer data from the whole sun month. *J. Geophys. Res.* 104, 9721–9726.
- Phillips, J.L., Balogh, A., Bame, S.J., Goldstein, B.E., Gosling, J.T., Hoeksema, J.T., McComas, D.J., Neugebauer, M., Sheeley, N.R., Wang, Y.M., 1994. ULYSSES at 50 deg south: constant immersion in the high-speed solar wind. *Geophys. Res. Lett.* 21, 1105–1108.
- Richter, I., Leinert, C., Planck, B., 1982. Search for short term variations of zodiacal light and optical detection of interplanetary plasma clouds. *Astron. Astrophys.* 110, 115–120.
- Sheeley Jr., N.R., Michels, D.J., Howard, R.A., Koomen, M.J., 1980. Initial observations with the Solwind coronagraph. *Astrophys. J.* 237, L99–L101.
- Tappin, S.J., Howard, T.A., 2009. Interplanetary coronal mass ejections observed in the heliosphere: 2. Model and data comparison. *Space Sci. Rev.* 147, 55–87.
- Tatarski, V.I., 1961. *Wave propagation in a Turbulent Medium*. McGraw-Hill, New York.
- Tokumaru, M., Kojima, M., Fujiki, M., Yamashita, M., 2003a. Global structure of interplanetary mass ejections retrieved from the model fitting analysis of radio scintillation observations. In: Velli, M., Bruno, R., Malara, F. (Eds.), *Proceedings of Solar Wind X*, AIP Conference Proceedings, vol. 679, pp. 729–732.
- Tokumaru, M., Kojima, M., Fujiki, K., Yamashita, M., Yokobe, A., 2003b. Toroidal-shaped interplanetary disturbance associated with the halo coronal mass ejection event on 14 July 2000. *J. Geophys. Res.* 108 (A5), 1220. doi:10.1029/2002JA009574.
- Tokumaru, M., Kojima, M., Fujiki, K., Yamashita, M., 2006. Tracking heliospheric disturbances by interplanetary scintillation. *Nonlin. Proc. Geophys.* 13, 329–338.
- Tokumaru, M., Kojima, M., Fujiki, K., Yamashita, Y., Jackson, B.V., 2007. The source and propagation of the interplanetary disturbance associated with the full-halo coronal mass ejection on 28 October 2003. *J. Geophys. Res.* 112, A05106. doi:10.1029/2006JA012043.
- Tokumaru, M., Kojima, M., Fujiki, K., 2010. Solar cycle evolution of the solar wind speed distribution from 1985–2008. *J. Geophys. Res.* 115, A04102. doi:10.1029/2009JA014628.
- Wagner, W.J., 1984. Coronal mass ejections. *Ann. Rev. Astron. Astrophys.* 22, 267–289.
- Wilson, D.C., 1977. NCAR Cooperative Thesis No. 40. Ph.D. Thesis, University of Colorado, Boulder, Colorado.
- Wood, B.E., Howard, R.A., Thernisien, A., Plunkett, S.P., Socker, D.G., 2009. Reconstructing the 3D Morphology of the 17 May 2008 CME. *Sol. Phys.* 259, 163–178.
- Worcester, P., Corunelle, B.D., Spindel, R.C., 1991. A review of ocean acoustic tomography: 1987–1990. *U.S. Natl. Rep. Int. Union Geod. Geophys. Rev. Geophys.* 29, 557–570.
- Wu, S.T., Dryer, M., Han, S.M., 1976. Interplanetary disturbances in the solar wind produced by density, temperature, or velocity pulses at 0.08 AU. *Sol. Phys.* 49, 187–204.
- Zidowitz, S., Inhester, B., Epple, A., 1996. Tomographic inversion of coronagraph images. In: Winterhalter, D., Gosling, J.T., Habbal, S.R., Kurth, W.S., Neugebauer, M. (Eds.), *Solar Wind Eight*, AIP Conference Proceedings, vol. 382. Woodbury, New York, pp. 165–168.